

Energy-Efficient Split Learning for Resource-Constrained Environments: A Smart Farming Solution

Keiwan Soltani*, Vishesh Kumar Tanwar*, Ashish Gupta†, Sajal K. Das*

*Department of Computer Science, Missouri University of Science and Technology, USA

†Department of Computer Science and Engineering, BITS Pilani Dubai Campus, UAE

Email: {ksoltani, vishesh.tanwar, sdas}@mst.edu, ashish@dubai.bits-pilani.ac.in

Abstract—Smart farming systems encounter significant challenges, including limited resources, the need for data privacy, and poor connectivity in rural areas. To address these issues, we present *eEnergy-Split*, an energy-efficient framework that utilizes split learning (SL) to enable collaborative model training without direct data sharing or heavy computation on edge devices. By distributing the model between edge devices and a central server, *eEnergy-Split* reduces on-device energy usage by up to 86% compared to federated learning (FL) while safeguarding data privacy. Moreover, SL improves classification accuracy by up to 6.2% over FL on ResNet-18 and by more modest amounts on GoogleNet and MobileNetV2. We propose an optimal edge deployment algorithm and a UAV trajectory planning strategy that solves the Traveling Salesman Problem (TSP) exactly to minimize flight cost and extend and maximize communication rounds. Comprehensive evaluations on agricultural pest datasets reveal that *eEnergy-Split* lowers UAV energy consumption compared to baseline methods and boosts overall accuracy by up to 17%. Notably, the energy efficiency of SL is shown to be model-dependent—yielding substantial savings in lightweight models like MobileNet, while communication and memory overheads may reduce efficiency gains in deeper networks. These results highlight the potential of combining SL with energy-aware design to deliver a scalable, privacy-preserving solution for resource-constrained smart farming environments.

Index Terms—Resource-constrained devices, Smart farming, Split learning, UAV, Edge computing.

I. Introduction

By 2050, global agriculture must nearly double its output to meet the demands of an estimated 9.7 billion people [1], [2]. While large farms are equipped to adopt advanced agriculture tools, small and medium-sized rural growers frequently lack the necessary infrastructure for the efficient implementation of available technologies (e.g., for pest detection) [3], [4]. Without timely interventions or accurate results, most farmers resort to excessive pesticide usage, degrading soil health, and contaminating water sources. Insights from our NSF I-Corps study [5] confirm the need for cost-effective, privacy-preserving technologies that remain functional in low-connectivity, resource-limited agricultural environments.

Unmanned aerial vehicles (UAVs) offer a promising solution to connectivity and data-processing limitations [6]–[8]. UAVs can operate as mobile sensing and computational platforms, bridging communication gaps and providing multi-sensory field data. By capturing localized pest activity and environmental conditions, UAVs reduce the reliance on centralized data aggregation, mitigating bandwidth constraints and latency issues. For instance, the authors in [9] proposed a trust-based scheme that ensures only reliable sensor data is collected, improving decision-making in pest management by filtering out faulty or malicious nodes. Moreover, the authors in [10] integrate trust mechanisms with energy-efficient data gathering in wireless sensor networks to enhance reliability and prolong network lifetime. While [11], [12] focused on affordability and energy-aware UAV deployment methods, their findings about minimizing the number of UAVs and leveraging reconfigurable intelligent surfaces are equally relevant to optimizing large-scale agricultural operations.

Further, from an aspect of Machine Learning (ML) with privacy preserving concerns, Federated Learning (FL) [13] has been adopted recently, which enables collaborative global model training without direct data sharing. However, it can burden resource-constrained devices by requiring local training of the entire model, potentially exposing them to privacy attacks. For example, the work [14] developed personalized FL frameworks to ensure that farms’ conditions—soil moisture, pest incidence, and crop phenotypes—are adequately captured without overburdening weaker devices or networks. On the communication front, techniques like collaborative FL [15] to reduce reliance on a central controller, and optimized FL algorithms focusing on resource allocation [16], demonstrate the network-aware learning strategies. Recent studies in UAV networks highlight the potential of integrating split learning (SL) [17], [18] with FL and reinforcement learning [19] to achieve enhanced scalability, accuracy, and energy efficiency. In SL, the model is partitioned between clients and a server to

reduce clients' computational burden. Liu et al. [20] presented a user scheduling approach that judiciously assigns participants to split or federated training modes to minimize energy consumption.

• **Motivation:** This research is motivated by the limitations of prior works: (i) *data privacy* – transmitting large volumes of raw data (collected by sensors deployed in farms) for remote model training is costly and raises privacy concerns; (ii) *UAV's energy constraints* – as UAVs run on battery, finding an optimized tour for data/model collection from the edge devices (sensors with computational capabilities) is still a challenge; (iii) overburdening the edge devices with intensive training of a complete ML model.

In this paper, while addressing the above limitations, we solve the problem: *how to build an ML-based agriculture solution with resource-constrained IoT devices while preserving data privacy*. As a solution, we propose an energy-efficient split learning based framework (abbreviated as **eEnergy-Split**).

• **Major Contributions:**

- We present a novel framework, eEnergy-Split, that facilitates model training by integrating a new method for optimal sensor deployment and an energy-aware UAV trajectory design using an exact Traveling Salesman Problem (TSP) solver, thereby minimizing the UAV's energy consumption and maximizing the number of completed communication rounds.
- The eEnergy-Split framework strategically integrates SL with FL by dividing the model into two parts—one residing on edge devices and the other on the server—thereby reducing the computational load on edge devices during model training.
- Through a series of insightful experiments, we evaluate the overall framework using benchmark models such as ResNet18, GoogleNet, and MobileNet V2, measuring metrics like energy consumption, CO₂ emissions, and accuracy. The results clearly show reduced energy usage, effectively extending network lifetime during incremental training.

Organization: Section II discusses the system model and problem formulation. Section III introduces the *eEnergy-Split* framework. We report the experimental results in Section IV. Finally, Section V concludes the paper with future research directions.

II. System Model and Problem Description

This section first describes the system along with the adopted energy model and then mathematically formulates the problem to be solved.

A. System Model

This work considers a wireless sensor network of N sensors $S = \{s_1, s_2, \dots, s_N\}$ uniformly distributed in

an agricultural field A . Each sensor records data (e.g., soil moisture, humidity, amount of minerals, images of insects, etc.) from the monitoring environment. This work considers two types of sensors: (i) the ones that capture data from the environment and (ii) the ones (also referred to as *edge devices*) that also have computational capabilities to process the collected data. Let $E = \{e_1, e_2, \dots, e_M\}$ be a set of M sensors of the latter type, where $E \subseteq S$ and $M \leq N$. Let (x_i, y_i) denote the coordinates of an IoT sensor s_i , for $1 \leq i \leq N$. Let $0 < \Delta_i \leq \Delta$ be the size of the recorded data by the sensor s_i . The distance (Euclidean) between s_i and s_j is denoted by d_{s_i, s_j} , and the sensors can communicate with each other within the Communication Range (CR) if $d_{s_i, s_j} \leq CR$. Similarly, the UAV can successfully collect data from an edge device e_i if $d_{UAV, e_i} \leq Rr$, where Rr is the reception range of the UAV. We assume that if the UAV hovers on top of an edge device, it can establish an acceptable communication. The UAV's data reception range Rr at altitude h is determined as $Rr = \sqrt{CR^2 - h^2}$ [21]. Note that the communication challenges, such as multi-path propagation, fading, or shadowing, are out of the scope of this work.

• **Energy Model for UAV:** The energy consumption of a UAV is determined by three primary components: (i) ξ_m — energy required for movement between hover points, (ii) ξ_h — the energy used to hover for data exchange, and (iii) ξ_c — the energy consumed for communication purposes. Let T_m, T_h , and T_c respectively denote the total movement time, total hovering time, and total communication time (for data gathering, uploading, and downloading model weights), needed to complete a single tour, where $T = T_m + T_h + T_c$. Moreover, the total energy utilized by the UAV during the mission must be less than its energy budget β , i.e., $T_m \cdot \xi_m + T_h \cdot \xi_h + T_c \cdot \xi_c < \beta$, where energy consumption components are computed for rotary-wing UAV [22] using Eq. (1) and Eq. (2).

$$\xi_m = P_0 \left(1 + \frac{3V^2}{U_{tip}^2}\right) + P_i \left(\sqrt{1 + \frac{V^4}{4v_0^4}} - \frac{V^2}{2v_0^2}\right)^{1/2} + \frac{1}{2} f \rho a V^3, \quad (1)$$

$$\xi_h = P_0 + P_i, \quad (2)$$

where $P_0 = \frac{\delta}{8} \rho a \Omega^3 R^3$ and $P_i = (1 + k) \frac{W^{3/2}}{\sqrt{2\rho a}}$, and P_0 and P_i represent the blade profile power and induced power, respectively. Table I shows the meaning and values for the other parameters that are selected based on the DJI Matrice 350 RTK, a widely used industrial-grade UAV known for its high endurance, stability, and advanced flight capabilities [23]. The reason for using the weight W in Newtons is to accurately represent the gravitational force acting on the UAV, as it is directly relevant to the power required for hovering and propulsion, which depend on force rather than mass. The weight W

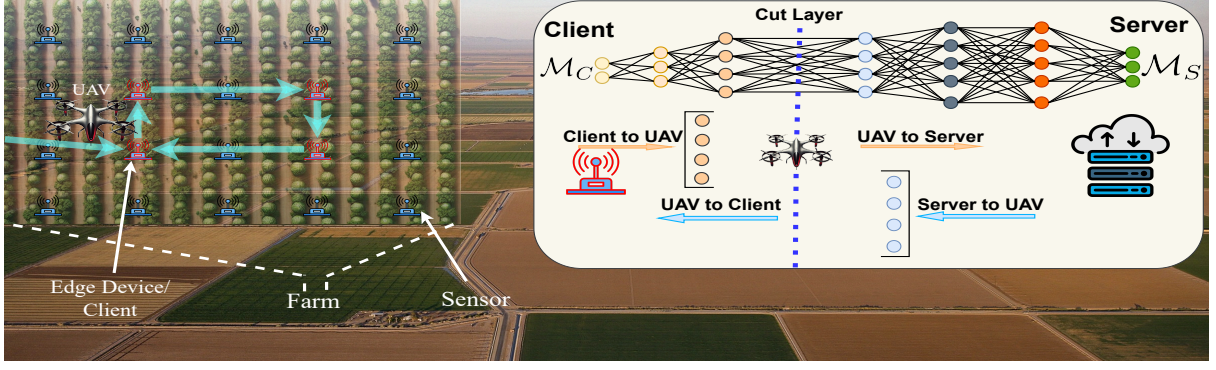


Fig. 1: The left sub-figure depicts a single farm with an example of the UAV trajectory for exchanging data with the cluster head devices (red-colored sensors). The right sub-figure illustrates the communication between a cluster head (client/edge device), a UAV, and a server.

can be calculated in Newtons using $W = m \cdot g$, where m is the mass in kilograms, and g is the acceleration due to gravity (9.81 m/s^2).

TABLE I: The parameters of the UAV energy model.

Parameters	Meaning	Value
β	UAV energy capacity	1.9 MJ
V	UAV speed	10 m/s
v_0	Mean motor induced velocity in hover	5.5 m/s
U_{tip}	Tip speed of the rotor blade	180 m/s
f	Fuselage drag ratio	0.8
r	Rotor solidity	0.08
ρ	Air density	1.225 kg/m ³
a	Rotor disc area	0.7 m ²
δ	Profile drag coefficient	0.011
Ω	Blade angular velocity	320 radians/s
R	Rotor radius	0.45 m
k	Incremental correction factor to induce power	0.15
W	Aircraft weight	63.4 Newton

• **Split Learning for Model Training:** Training deep learning models is computationally intensive, which can quickly drain the batteries of edge devices. Conversely, training on the cloud requires uploading all data, often necessitating numerous UAV tours that consume significant energy and shorten network lifetime. Therefore, reducing the computational burden of model training is essential, and SL offers a promising solution. In SL, training is divided: a portion is handled on the client side, while the remainder is done by a powerful cloud server. This paper considers a scenario where sensors periodically capture data from an agricultural field, and edge devices perform the client-side training. Due to communication constraints, these devices cannot directly forward their client-side smashed data or receive updated weights from the central server. Consequently, a UAV is employed to collect data from the edge devices, upload it to the cloud central server, and download the updated weights for broadcasting among the edge devices. The UAV facilitates this by traveling between predefined locations obtained strategically in the next section.

B. Problem Description

This research aims to jointly determine: (i) optimal positions for deploying edge devices to maximize data collection from the sensors and (ii) an efficient UAV trajectory that minimizes both the number of edge devices $|E|$ and the total UAV travel distance D_{UAV} , while maximizing the number of complete UAV tours, γ , over edge devices. The objective function as expressed in Eq. (3) considers normalized values of the concerned parameters. Eq. (4) enforces that the aggregation of the coverage of each edge device (e_i) captured as $C(e_i)$ covers entire set of the sensors deployed (S). At the same time, the UAV's energy constraint β as expressed in Eq (5) must be respected. In SL, the additional communication overhead for exchanging the raw and updated smashed data is denoted by T_{SL} . Formally, the optimization problem is defined as:

$$\min_{M, D_{UAV}, \gamma} M + D_{UAV} - \gamma, \quad (3)$$

$$\text{Subject to: } \bigcup_{e_i \in E} C(e_i) = S, \quad (4)$$

$$\xi_m + \xi_h + \xi_c < \beta, \quad (5)$$

$$\gamma = \left\lfloor \frac{\beta}{T_m \cdot \xi_m + T_h \cdot \xi_h + T_c \cdot \xi_c} \right\rfloor, \quad (6)$$

$$D_{UAV} = \sum_{i=1}^M d(e_i, e_{i+1}), \quad (7)$$

$$T_{SL} = \frac{L}{R} \quad (8)$$

In Eq. (6), the term $T_m \cdot \xi_m + T_h \cdot \xi_h + T_c \cdot \xi_c$ quantifies the total energy expenditure. Eq. (7) expresses the total travel distance for a UAV. In Eq. (8), L denotes the size of the smashed data generated by the partial model at the client, and R represents the effective data rate for UAV-edge communications.

III. eEnergy-Split Framework

In this section, we propose an energy-efficient split learning framework (**eEnergy-Split**) comprising three

major strategies for: (i) sensors and edge devices deployment, (ii) UAV trajectory design, (iii) SL based model training on edge devices. eEnergy-Split framework considers a UAV-assisted SL for precision agriculture scenarios, especially pest detection, with constrained connectivity and limited on-device resources. The overview of the framework is shown in Fig. 1, in which sensors collect data and hand over it to an edge device, on which a partial deep learning model \mathcal{M}_C (with the first few layers) is trained. Later, the ground truth, along with the client-side model weights, are offloaded to a UAV (visits periodically) that further delivers the received load to a server that hosts the remaining portion \mathcal{M}_S . The UAV operates as a mobile data relay between edge devices and the server. This paradigm reduces the computational burden on resource-limited devices and preserves data privacy while never exposing raw data.

A. Edge Devices Deployment

This section introduces an algorithm to deploy sensors (with limited hardware) and edge devices (sensors with computational resources like Jetson Nano) to optimize the overall data collection and model training process. Each edge device serves as a representative for a group of normal sensors and receives the collected data (image or other captured information from the field) from the sensors. To efficiently select and deploy edge devices, we propose an Algorithm 1.

In Algorithm 1, the deployment is achieved by prioritizing sensor nodes that provide the maximum coverage of their neighboring sensors within the communication range (CR). Using compressed sparse row (CSR) representation, the algorithm efficiently maintains adjacency information, significantly reducing memory usage and computational overhead. From the set of uncovered sensors, the sensor with the highest coverage degree is initially selected as an edge device. In the case of a tie, where multiple sensors cover the same number of uncovered nodes, the selection process further optimizes placement by choosing the sensor that minimizes the total distance to the already placed edge devices. This ensures an efficient distribution of edge devices across the network. Once an edge device is placed, all the uncovered sensors in its adjacency are removed from the uncovered set. The process continues iteratively until all sensors in the network are covered. The selected sensors as edge devices are the designated spots for client-side computation and UAVs' optimal hovering locations.

After the deployment of edge devices, the next crucial step is the assignment of sensors to their respective edge devices. This assignment must be optimized to balance the computational load and maintain efficient communication. Therefore, from Lines 22 to 27 of Algorithm 1, we introduce an optimized sensor-to-edge device assignment strategy.

Algorithm 1 Optimized Edge Device Deployment and Sensor Assignment using CSR

Require: Sensors $S = \{s_1, \dots, s_N\}$, communication_range CR

Ensure: Edge device positions and sensor assignments

- 1: Construct adjacency list \mathcal{A} with pair wise distances
- 2: $\mathcal{A}[s] \leftarrow \{u \mid d_{s,u} \leq CR, u \in S\}$ \triangleright stored in CSR format
- 3: $U \leftarrow \{s_1, s_2, \dots, s_N\}$ \triangleright Uncovered sensors
- 4: $E \leftarrow \emptyset$ \triangleright Edge device positions
- 5: **while** $U \neq \emptyset$ **do**
- 6: $\hat{\Delta} \leftarrow 0$ \triangleright Maximum coverage
- 7: $\hat{s} \leftarrow \text{None}$ \triangleright Best sensor for edge device
- 8: **for each** $s \in U$ **do**
- 9: $\hat{C} \leftarrow \mathcal{A}[s] \cap U$ \triangleright Covered sensors by s
- 10: **if** $|\hat{C}| > \hat{\Delta}$ **and** $E = \emptyset$ **then**
- 11: $\hat{\Delta} \leftarrow |\hat{C}|$
- 12: $\hat{s} \leftarrow s$
- 13: **else if** $|\hat{C}| \geq \hat{\Delta}$ **and** $E \neq \emptyset$ **and** $\sum d_{s,E} < \sum d_{\hat{s},E}$ **then**
- 14: $\hat{\Delta} \leftarrow |\hat{C}|$
- 15: $\hat{s} \leftarrow s$
- 16: **end if**
- 17: **end for**
- 18: $E \leftarrow E \cup \{\hat{s}\}$ \triangleright Place Edge device at \hat{s}
- 19: $U \leftarrow U \setminus \hat{C}$ \triangleright Update uncovered sensors
- 20: **end while**
- Assign Sensors to Edge Devices**
- 21: **for each** $s \in S \setminus E$ **do**
- 22: Identify candidate edge devices within CR from CSR adjacency list \mathcal{A}
- 23: Select edge device with minimal current load and shortest distance
- 24: Assign sensor s to this selected edge device
- 25: Update load distribution of edge devices
- 26: **end for**
- 27: **return** Edge devices E and sensor assignments

Time Complexity: Algorithm 1 iteratively examines all uncovered sensors, leading to a worst-case complexity of $O(N^2)$, where N is the number of sensors. The construction of the CSR-based adjacency list involves computing pairwise distances with a complexity of $O(N^2)$, which dominates the preprocessing phase.

B. Energy-Aware UAV Trajectory Design

This section presents an energy-aware UAV trajectory planning algorithm that determines the most efficient route for the UAV (i.e., path through the edge devices). After deployment, each sensor transmits its data to the assigned edge devices periodically. Once an edge device has received all data from its associated sensors, it performs client-side computation, i.e., partial model training. The computed model weights from edge devices, unable to directly reach the cloud server, are collected and relayed by a UAV for central training and aggregation. Subsequently, the UAV distributes the updated weights back to the devices for the next training iteration. To support this process, the UAV must follow

Algorithm 2 Energy-Constrained UAV Tour Planning Using Exact TSP Solver

Require: UAV's initial position O , edge device positions $E = \{e_1, e_2, \dots, e_M\}$, energy budget β , UAV speed V , movement energy ξ_m , hovering energy ξ_h , communication energy ξ_c

Ensure: Optimal UAV tour π , number of full rounds γ

- 1: Construct a complete distance graph G where nodes are E , edges are Euclidean distances between all device pairs
 - 2: Solve the exact TSP on G to find minimal tour π visiting all nodes in E
 - 3: Append the first node e_1 to the end of π to complete the tour
 - 4: **Energy and Round Initialization:**
 - 5: $D_\pi \leftarrow \text{Total tour length of } \pi$
 - 6: $\hat{E}_\pi \leftarrow \frac{D_\pi \cdot \xi_m}{V} + M \cdot (\xi_h + \xi_c) \triangleright$ Per round energy: move + hover + comm
 - 7: $e_1 \leftarrow \pi[0], e_M \leftarrow \pi[-2] \triangleright$ Start and last edge device in tour
 - 8: $\hat{E}_{\text{first}} \leftarrow \frac{d_{O, e_1} \cdot \xi_m}{V} + \hat{E}_\pi$
 - 9: $\hat{E}_{\text{return}} \leftarrow \frac{d_{e_M, O} \cdot \xi_m}{V} \triangleright$ Return energy
 - 10: $\gamma \leftarrow 0, \hat{\beta} \leftarrow \beta$
 - 11: **if** $\hat{E}_{\text{first}} + \hat{E}_{\text{return}} > \hat{\beta}$ **then**
 - 12: **return** $\pi, 0 \triangleright$ Insufficient energy for one full round
 - 13: **end if**
 - 14: $\hat{\beta} \leftarrow \hat{\beta} - \hat{E}_{\text{first}}$
 - 15: $\gamma \leftarrow 1$
 - 16: **while** $\hat{\beta} \geq \hat{E}_\pi + \hat{E}_{\text{return}}$ **do**
 - 17: $\hat{\beta} \leftarrow \hat{\beta} - \hat{E}_\pi$
 - 18: $\gamma \leftarrow \gamma + 1$
 - 19: **end while**
 - 20: **return** π, γ
-

an energy-efficient route to maximize the number of complete training rounds before needing to recharge.

Since UAVs are energy-constrained, optimizing their flight path is essential to maximizing the number of communication rounds they can perform before battery replacement or recharging is required. Because the number of edge devices is relatively small, we frame the UAV routing task as a classical TSP, aiming to find the shortest possible tour that visits all edge devices exactly once. Unlike heuristic-based solutions, we adopt an exact TSP solver that guarantees the globally optimal tour, minimizing the total flight distance. Although exact TSP has exponential worst-case complexity, our deployments involve only a few edge devices for farms up to 250 acres, enabling optimal routes to be computed almost instantly. For larger-scale scenarios, the method can be adapted to use heuristics to maintain near-optimal performance with practical runtimes.

The generated optimal tour π does not include the base station as a mandatory node. Instead, the UAV departs from the base station to the first edge device, traverses the TSP tour, and repeats the tour as many times as energy (β) permits without returning to base after each round. Before initiating a new round, the UAV checks

whether it has enough remaining energy to complete the next tour and return safely to the base station. If not, it aborts the next round and returns. This delayed-return strategy is incorporated in Algorithm 2, which captures the full energy-aware tour planning logic.

Algorithm 3 SL training in edge device-UAV framework

Require: Devices $E = \{e_1, \dots, e_M\}$ with model \mathcal{M}_C and dataset $\{D_e \in E\}$. Server with model \mathcal{M}_S , loss function \mathcal{L} , global aggregation rounds R , local split rounds r

Ensure: Updated \mathcal{M}_S and \mathcal{M}_C performance, consume energy

- 1: Initialize parameters for \mathcal{M}_C and \mathcal{M}_S
- 2: Initialize energy/time accumulators ($\mathcal{E}_{\text{total}}, T_{\text{total}}$)
- 3: **for** global_round = 1 **to** R **do**
- 4: **for** each client $e \in E$ and r rounds **do**
- 5: Obtain mini-batch (X, Y) from D_e
- 6: **// Client Forward Pass:**
- 7: $(\mathcal{E}_e^{\text{fwd}}, T_e^{\text{fwd}}) \leftarrow \text{EnergyTracker}$
- 8: Compute smashed data
- 9: **Record** T_e^{fwd} **and** $\mathcal{E}_e^{\text{fwd}}$
- 10: **// Server Forward Pass:**
- 11: Compute server output and loss
- 12: **// Distributed Backward Pass:**
- 13: $(\mathcal{E}_e^{\text{bwd}}, T_e^{\text{bwd}}) \leftarrow \text{EnergyTracker}$
- 14: Backpropagate ℓ through \mathcal{M}_S and \mathcal{M}_C
- 15: Update parameters in \mathcal{M}_S and \mathcal{M}_C
- 16: $\mathcal{E}_{\text{total}} \leftarrow \mathcal{E}_{\text{total}} + (\mathcal{E}_e^{\text{fwd}} + \mathcal{E}_e^{\text{bwd}})$
- 17: $T_{\text{total}} \leftarrow T_{\text{total}} + (T_e^{\text{fwd}} + T_e^{\text{bwd}})$
- 18: **end for**
- 19: **// Device's Model Aggregation across** E :

$$\theta_{\text{agg}} \leftarrow \frac{1}{M} \sum_{e \in E} \theta_e$$

- 20: Update each client e with θ_{agg}
 - 21: **end for**
 - 22: **return** Final model \mathcal{M} and $\mathcal{E}_{\text{total}}, T_{\text{total}}$
-

C. SL Training under eEnergy-Split Framework

Finally, the collaborative model training proceeds in alternating client (C) and server (S) side phases that the UAV orchestrates, as reported in Algorithm 3. At the beginning of each global round R , each edge device $e \in E$ holds a copy of the current client sub-model \mathcal{M}_C and a local mini-dataset D_e . The edge device selects a mini-batch $(X, Y) \subset D_e$, forwards the raw samples through \mathcal{M}_C , and produces the smashed representation Z to be handed over once the UAV arrives. The EnergyTracker routine records the time T_e^{fwd} and the energy $\mathcal{E}_e^{\text{fwd}}$ consumed by the device during computation and short-range transmission.

The UAV relays Z with the associated ground-truth labels to the server, where the remaining layers \mathcal{M}_S generate the predictions and the server performs its portion of back-propagation, returning the gradient concerning Z . Upon receipt, the edge device continues the backward pass through \mathcal{M}_C ; EnergyTracker again, measuring the client-side time T_e^{bwd} and the energy $\mathcal{E}_e^{\text{bwd}}$. Both sub-

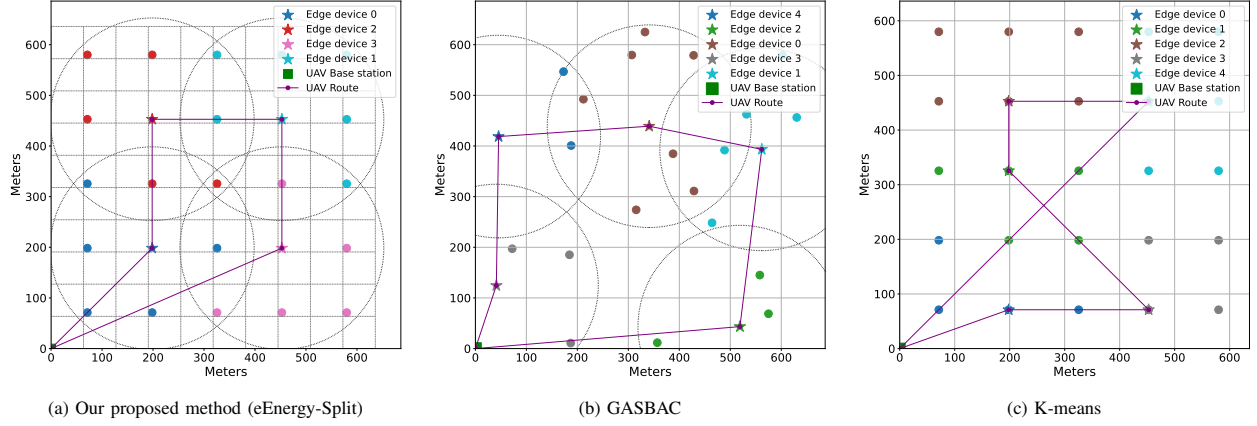


Fig. 2: Comparison of the three deployment strategies.

models then update their parameters using local optimizers, ensuring that computation remains split yet synchronous. Once each client has completed r such split rounds, the server aggregates the updated full-model (\mathcal{M}) weights with the arithmetic mean, θ_{agg} , and the UAV will broadcast to all devices during its next flight. The accumulators \mathcal{E}_{total} and T_{total} thus capture the complete resource footprint of forward computation, backward computation, and wireless transfer across the network. After the final round, the server holds the converged models ($\mathcal{M}_C, \mathcal{M}_S$).

IV. Experimental Evaluation

We evaluate the performance of our proposed algorithms in terms of sensor and edge devices deployment, energy consumption, and load distribution.

A. UAV Trajectories

Considering 25 sensors, with a communication range of 200 meters, deployed in a 100-acre farm, Fig. 2 demonstrates the deployment outcomes for eEnergy-Split (essentially Algorithm 1) and two baselines: Gathering data Assisted by Multi-UAV with a Balanced Clustering (GASBAC) [24] and K-means. GASBAC is a set of heuristic algorithms that balance energy consumption across sensor clusters and optimize UAV trajectories to extend the operational lifetime of wireless sensor networks in precision farming. In K-means, the value of K is initially set to $\lfloor \sqrt{N} \rfloor$ and incremented if any sensors remain unassigned. Once the edge devices and their corresponding sensor clusters are determined, the UAV follows a greedy approach to visit the edge devices. In Figs. 2a and 2c, sensors are uniformly deployed at a density of one sensor per five acres, while in Fig. 2b, sensors are randomly deployed. As shown in Fig. 2a, based on the communication range (CR), all sensors' data can be collected using the minimal number of edge devices while also minimizing the distances between them. Additionally, sensors are assigned to edge devices in a way that ensures an optimal workload distribution, enhancing overall efficiency.

B. UAV Energy Consumption

Next, we analyze the energy consumption of the UAV for a complete tour under different deployment scenarios. As shown in Table II, three distinct configurations are evaluated by varying the size of the agricultural field, the number of sensors, and the sensor-to-acreage ratio.

Across all configurations, eEnergy-Split framework consistently outperforms K-means and GASBAC in terms of UAV energy efficiency. Specifically, in the 100-acre scenario, the UAV consumes only 35.1 kilojoules (kJ) using our approach, compared to 80.89 kJ and 92.80 kJ for K-means and GASBAC, respectively. This corresponds to a reduction of approximately 56.6% and 62.2% in energy consumption. Similarly, in the 140-acre field with 36 sensors, our method reduces energy use to 57.68 kJ, which is about 50% and 51% lower than K-means and GASBAC, respectively. In the most demanding 200-acre scenario with 49 sensors, the UAV energy consumption using our method is 103.10 kJ, significantly less than the 154.19 kJ for K-means and 164.37 kJ for GASBAC.

TABLE II: Energy in Joules (J) Consumption Analysis

Configuration			UAV Energy Consumption (kJ/Trip)		
Farm Acres	# Sensors	Sensor per # Acres	eEnergy-Split	K-means	GASBAC
100	25	5	35.07	80.89	92.80
140	36	4	57.68	114.96	117.33
200	49	8	103.10	154.19	164.37

On average, our proposed method decreases UAV energy consumption by approximately 50% compared to K-means and by 60% compared to GASBAC. These improvements can be attributed to optimized edge device placement and sensor assignment strategies used in eEnergy-Split, which result in shorter UAV flight paths and more efficient data aggregation. In contrast, GASBAC, originally designed for multi-UAV systems, incurs higher overhead when adapted to a single UAV, while K-means suffers from suboptimal cluster formation. Overall, eEnergy-Split gives the most energy-efficient and scalable solution among the evaluated approaches.

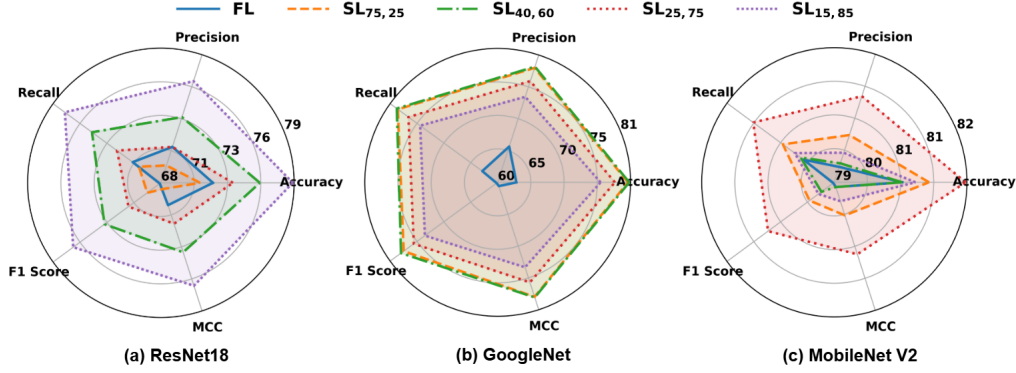


Fig. 3: Radar charts comparing evaluation metrics on the KAP dataset for different architectures and SL variations. Higher values closer to the outer edge indicate better performance. Note: $SL_{a,b}$ denotes that the client has $a\%$ of layers and the server has the remaining $b\%$ of layers.

C. Performance Analysis

We implement all experiments in *Python 3* using PyTorch, utilizing an Nvidia RTX A5000 GPU, 8 CPU cores @1.5 GHz (FP32 \approx 27.8 TFLOPS), 768 GB/s, tensor FLOPS \approx 216 TFLOPS, CPU PassMark \approx 35000, and 40 GB of system memory. We performed our experiments on three DNN architectures: ResNet18 (RN) [25], GoogleNet (GN) [26], and MobileNetV2 (MN) [27] on Kaggle’s Agriculture Pests (KAP) image dataset [28], having 12 pest species, namely, ants, bees, beetles, caterpillars, moths, earthworms, earwigs, grasshoppers, slugs, snails, wasps, and weevils. We partition the training dataset into training (90%) and validation (10%), and report the results of the test dataset, and images are resized to (224, 224). We split each model into four sub-models to simulate the SL in low-configured edge devices (with 15%, 25%, 40%, and 75% of the layers, and the remainder is over the server) and compare client and server computational loads with different cut layers.

Hyperparameter and Data Heterogeneity: We consider four clients and assign data of 3 classes to each to simulate a non-IID distribution. We use the cross-entropy loss function, the AdamW optimizer, and evaluate on metrics such as accuracy, precision, recall, F1-score, and Matthews Correlation Coefficient (MCC). Fig. 3 compares the classification performance of FL and SL across three backbone architectures: ResNet-18 (a), GoogleNet (b), and MobileNetV2 (c). For SL, we vary the fraction of layers hosted on the client from 75% down to 15% (i.e., $SL_{75,25}$ in orange dashed, $SL_{40,60}$ in green dash-dot, $SL_{25,75}$ in red dotted, and $SL_{15,85}$ in purple dotted).

For **ResNet-18**, the FL baseline attains 72.34% accuracy, $F1 = 0.684$, and $MCC = 0.701$. Leveraging SL yields steady gains as more layers move server-side: the orange dashed trace ($SL_{75,25}$) shows 71.34% accuracy (−1.0 percentage point (pp) vs. FL), $F1 = 0.697$, and $MCC = 0.688$; the green dash-dot curve ($SL_{40,60}$) rises to 75.98% (+3.6 pp), $F1 = 0.736$, and $MCC = 0.739$; the red dotted line ($SL_{25,75}$) gives 73.89% (+1.6 pp), $F1 = 0.712$, and $MCC = 0.716$; and the purple dotted trace ($SL_{15,85}$)

achieves the best performance with 78.53% (+6.2 pp), $F1 = 0.765$, and $MCC = 0.766$. Thus, $SL_{15,85}$ (purple) exceeds FL by over 6% in accuracy and at least 8% F1.

For **GoogleNet**, the FL baseline delivers only 63.15% accuracy, $F1 = 0.605$, and $MCC = 0.609$, whereas the red dotted trace ($SL_{25,75}$) jumps to 80.35% (+17.2 pp), $F1 = 0.785$, and $MCC = 0.786$. Both the purple dotted ($SL_{15,85}$, 80.16% Acc, $F1 = 0.780$, $MCC = 0.785$) and green dash-dot ($SL_{40,60}$, 78.16% Acc, $F1 = 0.761$, $MCC = 0.762$) remain above FL, confirming that GoogleNet’s inverted-residual design is highly amenable to SL.

In the case of **MobileNetV2**, we begin from a strong FL baseline of 80.62% accuracy, $F1 = 0.788$, and $MCC = 0.789$. $SL_{75,25}$ further improves to 81.35% (+0.73 pp), $F1 = 0.796$, and $MCC = 0.797$. $SL_{40,60}$ (green dash-dot line) holds steady at 80.62% accuracy, $F1 = 0.792$, and $MCC = 0.789$, whereas $SL_{25,75}$ achieves the peak performance with 82.35% accuracy (+1.73 pp), $F1 = 0.810$, and $MCC = 0.808$. Finally, $SL_{15,85}$ delivers 80.98% accuracy (+0.36 pp), $F1 = 0.793$, and $MCC = 0.793$, nearly matching the FL baseline.

These results demonstrate that SL, when the server hosts at least 60% of layers, can consistently match or outperform FL on all three architectures. Moreover, the optimum split point varies by backbone (most server-heavy for ResNet-18 and GoogleNet, intermediate for MobileNetV2), illustrating how SL enables a fine-grained trade-off between client computing, privacy exposure, and end-to-end accuracy.

D. Resource Efficiency Analysis

We estimate the execution time on a low-powered edge device (Jetson AGX Orin [29]) by scaling our measured times on an NVIDIA RTX A5000 according to key hardware metrics. Specifically, we account for differences in FP32 throughput (FLOPS), memory bandwidth (MemBW), tensor-core performance (TFLOPS), CPU capability, software factor (SF), and optimization factor (OF). We measured the source device timing T_{src} on

RTX A5000 and estimated timing T_{tgt} on Jetson as:

$$T_{tgt} = T_{src} \times \left(\frac{FLOPS_{src}}{FLOPS_{tgt}} \right)^{w_1} \times \left(\frac{MemBW_{src}}{MemBW_{tgt}} \right)^{w_2} \times \left(\frac{TFLOPS_{src}}{TFLOPS_{tgt}} \right)^{w_3} \times \left(\frac{CPU_{src}}{CPU_{tgt}} \right)^{w_4} \times SF \times OF, \quad (9)$$

where $w_1 = 1.0$, $w_2 = 0.5$, $w_3 = 0.8$, $w_4 = 0.3$, $SF = OF = 1$. For simulation, we consider Jetson AGX Orin having 2048 CUDA cores, @1.3 GHz (FP32 \approx 2.7 TFLOPS), 51.2 GB/s, tensor FLOPS \approx 21.6 TFLOPS, and CPU PassMark \approx 2500. We assumed that the time on RTX A5000 was measured under identical software and batch sizes. Energy and CO₂ emissions on Jetson are considered to be proportional to execution time. The server remains on RTX A5000; only client times are down-scaled to Jetson. We reported the average time, energy consumption, and CO₂ emissions for client (C) and server (S) in FL and four SL splits (please ref. Section IV-C) in Table III.

For **ResNet-18**, FL (Accuracy 72.34%) places almost all cost on the client, namely computation time of 133.7 seconds, energy consumption of \approx 20kJ, and 2.6g of CO₂ emission, while server cost is negligible (Table III(a)). However, SL_{15,85} that computes only 15% of layers on farm devices and slashes client time to 14 seconds (89.5% reduction from FL) at the expense of raising client energy in the range [31.23, 42.79]kJ and CO₂ to \approx 5g and increasing server use to 0.393 seconds, energy to 0.086kJ, and CO₂ emission to 0.01135g. Intermediate splits such as SL_{40,60} achieved 75.98% accuracy and report client time as 35 seconds and server time as 0.241 seconds, with moderate energy consumption and CO₂ emission trade-offs.

For **GoogleNet**, FL achieved 63.15% accuracy and again burdens the farm devices with computation time (195 ± 21) seconds, energy consumption in the range of [24.9, 30.4], CO₂ emission of \approx 4 g, and barely taxes the server (Table III(b)). The SL_{25,75} split achieved an accuracy of 80.35%; however, the farm device/client latency falls to 52.19 ± 2.14 seconds, client energy to 60.97 ± 14.81 kJ, and CO₂ to 10g (approx), while server costs double relative to the FL approach. Even SL_{40,60} (accuracy = 78.16%) took computational time of around 58 seconds and consumes the median energy of 61.34kJ.

For **MobileNetV2** architecture, the SL_{15,85} split maintains 80.98% accuracy while reducing client time to 26.50 seconds and energy to 4.50 ± 1.02 kJ (CO₂ = 0.59 g), with server time and energy consumption rising to 0.493 seconds and 0.0596kJ respectively, as shown in Table III (c). Another split, SL_{25,75}, achieved an accuracy of 82.35% and further cuts on-device computational time and CO₂, demonstrating that modest offloading over the cloud can even improve accuracy while drastically lowering edge resource demands.

TABLE III: Average Time, Energy, and CO₂ Emission by Client (C) and Server (S).

(a) ResNet18

Method	Time (s)		Energy (kJ)		CO ₂ (g)	
	C	S	C	S	C	S
FL	133.70 \pm 0.04	0.137	19.65 \pm 1.55	0.028	2.59 \pm 0.20	0.0037
SL _{75,25}	41.12 \pm 0.53	0.204	43.28 \pm 11.01	0.0649	5.71 \pm 1.45	0.0086
SL _{40,60}	34.99 \pm 0.15	0.241	42.09 \pm 11.33	0.0653	5.55 \pm 1.49	0.0086
SL _{25,75}	27.91 \pm 0.22	0.297	47.47 \pm 14.32	0.0374	6.26 \pm 1.89	0.0049
SL _{15,85}	13.58 \pm 0.43	0.393	37.01 \pm 5.78	0.086	4.88 \pm 0.77	0.0114

(b) GoogleNet

Method	Time (s)		Energy (kJ)		CO ₂ (g)	
	C	S	C	S	C	S
FL	194.76 \pm 20.45	0.210	27.62 \pm 2.74	0.038	3.65 \pm 0.36	0.0050
SL _{75,25}	69.55 \pm 1.09	0.360	60.34 \pm 14.49	0.217	7.96 \pm 1.91	0.0286
SL _{40,60}	56.73 \pm 1.86	0.450	61.34 \pm 17.30	0.214	8.09 \pm 2.28	0.0283
SL _{25,75}	52.19 \pm 2.14	0.480	60.97 \pm 14.81	0.227	8.04 \pm 1.95	0.0300
SL _{15,85}	39.04 \pm 1.73	0.560	63.08 \pm 21.72	0.235	8.32 \pm 2.87	0.0311

(c) MobileNet

Method	Time (s)		Energy (kJ)		CO ₂ (g)	
	C	S	C	S	C	S
FL	196.01 \pm 0.32	0.167	32.96 \pm 1.68	0.033	0.43 \pm 0.02	0.0043
SL _{75,25}	65.10 \pm 0.06	0.260	7.93 \pm 1.84	0.039	1.05 \pm 0.24	0.0051
SL _{40,60}	51.95 \pm 0.06	0.333	6.80 \pm 1.93	0.048	0.90 \pm 0.25	0.0065
SL _{25,75}	42.68 \pm 0.04	0.360	7.00 \pm 1.78	0.035	0.92 \pm 0.23	0.0046
SL _{15,85}	26.50 \pm 0.03	0.493	4.50 \pm 1.02	0.060	0.59 \pm 0.13	0.0079

We observed that SL consistently reduces execution time on the client side across all models; however, it is not directly proportional to reductions in energy consumption and CO₂ emissions. In ResNet18 and GoogleNet, for example, client time drops significantly with SL splits while the energy/emissions increase in some cases than FL. This counterintuitive behavior arises because SL introduces multiple forward and backward passes at shallower layers that can be computationally inefficient. These layers often involve high-resolution feature maps and large memory footprints, which incur greater energy costs even for short execution times. Moreover, frequent data exchange with UAV also increases the energy overhead. In contrast, MobileNetV2, with its lightweight inverted residual structure, handles early-layer computations more efficiently, allowing SL to reduce both time and energy simultaneously. This highlights that model architecture is crucial in determining whether SL yields energy savings or trade-offs.

V. Conclusion

In this paper, we introduced *eEnergy-Split*, an energy-aware framework that combines split learning (SL) with an optimal sensor deployment strategy and a UAV path planning method based on an exact TSP solver. The proposed framework enables efficient and privacy-preserving collaborative learning across edge devices in smart farming environments. By partial offloading to the server, *eEnergy-Split* significantly reduces on-device

energy consumption and improves model accuracy compared to FL. Extensive experiments on the pest dataset demonstrate that SL improves classification performance while lowering UAV energy consumption, supporting longer mission durations. Notably, our findings reveal that the energy efficiency of SL is model-dependent. MobileNetV2 achieves significant reductions in energy use and CO_2 emissions compared to ResNet18 and GoogleNet. These results emphasize the importance of aligning model architecture with system-level design choices to maximize the benefits of SL in resource-constrained environments. Future research will focus on reducing communication overhead in SL through activation compression and sparsification techniques. We also plan to explore adaptive split point selection based on real-time energy profiling and network conditions. Furthermore, we intend to develop a full hardware prototype and deploy it in an actual farm environment, creating a real-world testbed to conduct live experiments and validate the framework's performance through real-time analysis under practical conditions.

Acknowledgments: This work is supported by the NSF award #s 2331554 (I-Corps), SCC-1952045 (SIRAC), PFI-RP-2431990, AI-ENGAGE-2520346 (HARVEST).

References

- [1] S. A. Bhat and N.-F. Huang, "Big data and ai revolution in precision agriculture: Survey and challenges," *IEEE Access*, vol. 9, pp. 110209–110222, 2021.
- [2] D. K. Ray, N. D. Mueller, P. C. West, and J. A. Foley, "Yield trends are insufficient to double global crop production by 2050," *PloS one*, vol. 8, no. 6, p. e66428, 2013.
- [3] A. Albanese, M. Nardello, and D. Brunelli, "Automated pest detection with dnn on the edge for precision agriculture," *IEEE Journal on Emerging and Selected Topics in Circuits and Systems*, vol. 11, no. 3, pp. 458–467, 2021.
- [4] M. C. F. Lima, M. E. D. de Almeida Leandro, C. Valero, L. C. P. Coronel, and C. O. G. Bazzo, "Automatic detection and monitoring of insect pests—a review," *Agriculture*, vol. 10, no. 5, p. 161, 2020.
- [5] V. Tanwar, "I-Corps: Bugs-B-Gone: Developing a robust and automated insect detection system for connecting farm communities," in *NSF Award # 2331554*, 2023.
- [6] C. Lin, G. Han, X. Qi, J. Du, T. Xu, and M. Martínez-García, "Energy-optimal data collection for unmanned aerial vehicle-aided industrial wireless sensor network-based agricultural monitoring system: A clustering compressed sampling approach," *IEEE Transactions on Industrial Informatics*, vol. 17, no. 6, pp. 4411–4420, 2020.
- [7] A. Caruso, S. Chessa, S. Escolar, J. Barba, and J. C. López, "Collection of data with drones in precision agriculture: Analytical model and lora case study," *IEEE Internet of Things Journal*, vol. 8, no. 22, pp. 16692–16704, 2021.
- [8] P. Velusamy, S. Rajendran, R. K. Mahendran, S. Naseer, M. Shafiq, and J.-G. Choi, "Unmanned aerial vehicles (uav) in precision agriculture: Applications and challenges," *Energies*, vol. 15, no. 1, p. 217, 2021.
- [9] B. Jiang, G. Huang, T. Wang, J. Gui, and X. Zhu, "Trust based energy efficient data collection with unmanned aerial vehicle in edge network," *Transactions on Emerging Telecommunications Technologies*, vol. 33, no. 6, p. e3942, 2022.
- [10] K. Soltani, L. Farzinavash, and M. A. Balafar, "Trust-aware and energy-efficient data gathering in wireless sensor networks using pso," *Soft Computing*, vol. 27, pp. 11731–11754, 2023.
- [11] W. Xu, T. Xiao, J. Zhang, W. Liang, Z. Xu, X. Liu, X. Jia, and S. K. Das, "Minimizing the deployment cost of uavs for delay-sensitive data collection in iot networks," *IEEE/ACM Transactions on Networking*, vol. 30, no. 2, pp. 812–825, 2021.
- [12] D. Tyrovolas, P.-V. Mekikis, S. A. Tegos, P. D. Diamantoulakis, C. K. Liaskos, and G. K. Karagiannidis, "Energy-aware design of uav-mounted ris networks for iot data collection," *IEEE Transactions on Communications*, vol. 71, no. 2, pp. 1168–1178, 2022.
- [13] D.-D. Le, M.-S. Dao, A.-K. Tran, T.-B. Nguyen, and H.-G. Le-Thi, "Federated learning in smart agriculture: An overview," in *International Conference on Knowledge and Systems Engineering*. IEEE, 2023, pp. 1–4.
- [14] W. Wu, M. Li, K. Qu, C. Zhou, X. S. Shen, W. Zhuang, X. Li, and W. Shi, "Split learning over wireless networks: Parallel design and resource management," *IEEE Journal on Selected Areas in Communications*, vol. 41, pp. 1051–1066, 2022.
- [15] M. Chen, H. V. Poor, W. Saad, and S. Cui, "Wireless communications for collaborative federated learning," *IEEE Communications Magazine*, vol. 58, pp. 48–54, 2020.
- [16] V.-D. Nguyen, S. K. Sharma, T. X. Vu, S. Chatzinotas, and B. E. Ottersten, "Efficient federated learning algorithm for resource allocation in wireless iot networks," *IEEE Internet of Things Journal*, vol. 8, pp. 3394–3409, 2021.
- [17] X. Liu, Y. Deng, and T. Mahmoodi, "A novel hybrid split and federated learning architecture in wireless uav networks," in *IEEE International Conference on Communications*, 2022, pp. 1–6.
- [18] C. Thapa, P. C. M. Arachchige, S. Camtepe, and L. Sun, "Splitfed: When federated learning meets split learning," in the *AAAI Conference on Artificial Intelligence*, vol. 36, no. 8, 2022, pp. 8485–8493.
- [19] V. K. Tanwar, S. Sarkar, A. K. Singh, and S. K. Das, "Reind-split: Reinforced dynamic split learning for pest recognition in precision agriculture," *arXiv preprint arXiv:2506.13935*, 2025.
- [20] X. Liu, Y. Deng, and T. Mahmoodi, "Energy efficient user scheduling for hybrid split and federated learning in wireless uav networks," in *IEEE International Conference on Communications*, 2022, pp. 1–6.
- [21] K. Soltani, F. Coro, and S. K. Das, "Optimizing uav-assisted data collection in iot sensor networks using dual cluster head strategy," in *IEEE 21st International Conference on Mobile Ad-Hoc and Smart Systems (MASS)*, 2024, pp. 279–287.
- [22] Y. Zeng, J. Xu, and R. Zhang, "Energy minimization for wireless communication with rotary-wing uav," *IEEE Transactions on Wireless Communications*, vol. 18, no. 4, pp. 2329–2345, 2019.
- [23] DJI, *Matrice 350 RTK User Manual*, 2023. [Online]. Available: https://dl.djicdn.com/downloads/matrice_350_rtk/Matrice_350_RTK_User_Manual_en.pdf
- [24] K.-V. Nguyen, C.-H. Nguyen, T. V. Do, and C. Rotter, "Efficient multi-uav assisted data gathering schemes for maximizing the operation time of wireless sensor networks in precision farming," *IEEE Transactions on Industrial Informatics*, vol. 19, no. 12, pp. 11664–11674, 2023.
- [25] K. He, X. Zhang, S. Ren, and J. Sun, "Deep residual learning for image recognition," in *IEEE Conference on Computer Vision and Pattern Recognition*, 2016, pp. 770–778.
- [26] C. Szegedy, W. Liu, Y. Jia, P. Sermanet, S. Reed, D. Anguelov, D. Erhan, V. Vanhoucke, and A. Rabinovich, "Going deeper with convolutions," in *IEEE Conference on Computer Vision and Pattern Recognition*, 2015, pp. 1–9.
- [27] M. Sandler, A. Howard, M. Zhu, A. Zhmoginov, and L.-C. Chen, "Mobilenetv2: Inverted residuals and linear bottlenecks," in *IEEE Conference on Computer Vision and Pattern Recognition*, 2018, pp. 4510–4520.
- [28] Kaggle, "Agricultural Pests Image Dataset," <https://www.kaggle.com/datasets/vencerlanz09/agricultural-pests-image-dataset>, [Online; accessed April 22, 2025].
- [29] NVIDIA, "Jetson AGX Orin Series," <https://www.nvidia.com/content/dam/en-zz/Solutions/gtc/t21/jetson-orin/nvidia-jetson-agx-orin-technical-brief.pdf>.